JOURNAL OF SPACECRAFT AND ROCKETS
Vol. 42, No. 5, September–October 2005

Lateral Motion of Free-Rolling Tail Rockets in Free Flight

J. Morote*
National Institute of Aerospace Technology, 28850 Madrid, Spain

A study of the dynamics of free-rolling tail configurations is presented. The linearized theory of symmetric missiles motion is extended to free-rolling tail configurations to define a dynamically equivalent fixed-tail rocket. The asymmetries effect is introduced by small forcing functions at body and tail roll rate frequencies. Finally, Magnus effects and conditions at resonance and resonance lock-in are discussed.

Nomenclature

C_D = drag force coefficient
$C_{L\alpha}$ = lift force coefficient slope
C_{li} = induced roll moment coefficient
C_{lp} = roll damping moment coefficient
$C_{l\delta T}$ = roll effectiveness moment coefficient
$C_M e^{i\phi_M}$ = complex moment coefficient, $Cm + iCn$
$C_{MB,T0} e^{i\phi_{M0}}$ = asymmetry moment coefficient
$C_{mp\alpha}$ = Magnus moment coefficient
C_{mq}, $C_{m\dot{\alpha}}$ = pitch damping moment derivatives
$C_{m\alpha}$ = pitching moment coefficient slope
$C_N e^{i\phi_N}$ = complex force coefficient, $Cy + iCz$
$C_{NB,T0} e^{i\phi_{N0}}$ = asymmetry force coefficient
C_{Npq}, $C_{Np\dot{\alpha}}$ = pitch–yaw force derivatives
C_{Nq}, $C_{N\dot{\alpha}}$ = pitch–yaw force derivatives
$C_{N\dot{q}}$, $C_{Np\dot{q}}$ = pitch–yaw force derivatives
$C_{Np\alpha}$ = Magnus force coefficient
$C_{N\alpha}$ = normal force coefficient slope
$C^*_{\square}$ = $C_{\square}(\rho SD/2m)$
$C^*_{\square B,T}$ = $C_{\square B,T}(\rho SD/2m_{B,T})$
D = reference length, missile diameter
g = gravity acceleration
I_x = global axial moment of inertia
$I_{xB,T}$ = body or tail axial moment of inertia
I_y = transversal moment of inertia
k_a = axial radii of gyration
k_t = transverse radii of gyration
l_B = dimensionless distance between body and global c.g.
l_{BT} = dimensionless distance between body and tail c.g.
l_T = dimensionless distance between tail and global c.g.
m = mass
$p_{B,T}$ = body or tail roll rate
q = pitch rate
q_d = dynamic pressure
r = yaw rate
$\hat{r}$ = radial offset of c.m.
S = reference area, $\pi D^2/4$
s = dimensionless arclength, $\int_{to}^{t} (V/D)\,\mathrm{d}t$
t = time
u = X-velocity component
V = missile speed
v = Y-velocity component
w = Z-velocity component
α, β = angles of attack and sideslip
γ = u/V
δ = fin cant angle
Θ = angle between the longitudinal axis and the horizontal
$\iota_{B,T}$ = $I_y/I_{yB,T}$
κ = bearing friction moment coefficient
λj = damping rates
μ = $(q + i\,r)D/V$
$\xi_{B,T}$ = steady-state trim angles for body or tail asymmetries
$\xi_{b,t}$ = $\tilde{\xi}$ in body- or tail-fixed axes
$\tilde{\xi}$ = $\tilde{\beta} + i\tilde{\alpha}$ complex angle of attack in nonrolling axes system, $(v + iw)/V$
ρ = density
σ = I_x/I_y
$\sigma_{B,T}$ = $I_{xB,T}/I_y$
ϕ = roll angle, $\int_{to}^{t} p\,\mathrm{d}t$
$\phi'_{B,T}$ = dimensionless body or tail roll rates, $p_{B,T}D/V$
ϕ'_j = modal frequencies

Subscripts

B = body
e = steady
F = fixed-tail configuration
g = gyroscopically equivalent
m = Magnus equivalent
r = resonance
st = static
T = tail

Superscripts

$\cdot$ = differentiation with respect to t
$'$ = differentiation with respect to s
$\tilde{}$ = nonrolling axes

Introduction

THE free-rolling tail concept is a practical means of reducing unwanted roll control reversals in canard-controlled missiles at low angles of attack.[1] A freely spinning stabilizer immersed in the canard downwash flowfield does not transmit undesirable induced roll moments to the body. Experimental wind-tunnel investigations[2] were conducted, and several designs present this configuration [MAGIC R.550 and Guided Multiple Launch Rocket System (GMLRS)].

Presented as Paper 2004-5056 at the AIAA Atmospheric Flight Mechanics Conference, Providence, RI, 16–19 August 2004; received 20 September 2004; revision received 19 November 2004; accepted for publication 19 November 2004.

*Research Engineer, Aerodynamics Branch. Member AIAA.

The free-rolling tail arrangement was proposed[3] to reduce dispersion due to the manufacturing tolerances of ballistic configurations, while lessening instabilities such as roll resonance and the catastrophic yaw associated with fixed-cruciform stabilizers. Free-rolling tails on non-maneuvering missile systems and free-fall stores were both wind-tunnel and free-flight tested.[3,4]

This paper presents a study of the dynamics of slightly unsymmetrical free-rolling tail configurations and defines a dynamically equivalent fixed-tail missile. The free-rolling tail separates body and tail lock-in occurrence, which may improve the performance of some types of vehicles. The coupling introduced by the bearing friction and the effect of proximity between rates can affect body or tail lock-in at a faster timescale than that associated with changes in environmental conditions.

Equations of Motion

The lateral motion of a free-rolling tail rocket may be described by two rigid solids with mutual interaction consisting of a transverse force and a moment. The two vectorial equations for the body in an inertial coordinate system are

$$m_B\dot{\boldsymbol{V}}_B = \boldsymbol{F}_A + m_B\boldsymbol{g} + \boldsymbol{F}_{\mathrm{TB}} \tag{1a}$$

$$\dot{\boldsymbol{H}}_B = \boldsymbol{M}_A + \boldsymbol{M}_{\mathrm{TB}} \tag{1b}$$

where $\boldsymbol{F}_A$ and $\boldsymbol{M}_A$ are the aerodynamic force and moment and $\boldsymbol{F}_{TB}, \boldsymbol{M}_{TB}$ are the interactions of force and moment between the tail and body.

In a body-fixed system of axes at the body's c.g., where X is the centerline of the body positive forward, Y is perpendicular to plane of symmetry positive to the right when looking forward, and Z is perpendicular to both the X and Y axes positive downward, and under the assumption of mass rotational symmetry, products of inertia zero and horizontal flight, the main vectors are

$$\boldsymbol{V}_B = (u_B, v_B, w_B) \tag{2a}$$

$$\boldsymbol{\Omega}_B = (p_B, q_B, r_B) \tag{2b}$$

$$\boldsymbol{g} = (0, g_y, g_z) \tag{2c}$$

$$\boldsymbol{H}_B = (I_{xB}p_B, I_{yB}q_B, I_{yB}r_B) \tag{2d}$$

For a nonrolling coordinate system at the body's c.g. $X'Y'Z'$ (Fig. 1), where the velocity is $(u_B, \tilde{v}_B, \tilde{w}_B)$, the angular velocity is $(p_B, \tilde{q}_B, \tilde{r}_B)$, and the angular velocity of the coordinate system is $(0, \tilde{q}_B, \tilde{r}_B)$, the four transverse components derived from the vectorial equations are

$$\dot{\tilde{v}}_B + u_B\tilde{r}_B = \left(\frac{\rho SV^2}{2m_B}\right)\tilde{C}_{yB} + \tilde{g}_y + \frac{\tilde{F}_{Y\mathrm{TB}}}{m_B} \tag{3a}$$

$$\dot{\tilde{w}}_B - u_B\dot{\tilde{q}}_B = \left(\frac{\rho SV^2}{2m_B}\right)\tilde{C}_{zB} + \tilde{g}_z + \frac{\tilde{F}_{Z\mathrm{TB}}}{m_B} \tag{3b}$$

$$\dot{\tilde{q}}_B + \frac{I_{xB}}{I_{yB}}p_B\tilde{r}_B = \left(\frac{\rho SV^2D}{2I_{yB}}\right)\tilde{C}_{mB} + \frac{\tilde{F}_{Z\mathrm{TB}}l_{\mathrm{BT}}D}{I_{yB}} + \frac{\tilde{M}_Y}{I_{yB}} \tag{3c}$$

$$\dot{\tilde{r}}_B - \frac{I_{xB}}{I_{yB}}p_B\tilde{q}_B = \left(\frac{\rho SV^2D}{2I_{yB}}\right)\tilde{C}_{nB} - \frac{\tilde{F}_{Y\mathrm{TB}}l_{\mathrm{BT}}D}{I_{yB}} + \frac{\tilde{M}_Z}{I_{yB}} \tag{3d}$$

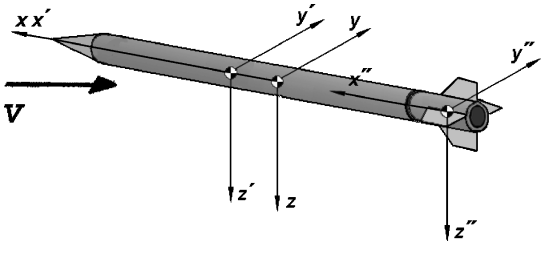

Fig. 1 Nonrolling systems of axes.

where the aerodynamic force and moment components were expressed in the usual dimensionless form. When time is replaced by dimensionless distance as an independent variable,

$$\dot{V} = \frac{\mathrm{d}V}{\mathrm{d}t} = \frac{\mathrm{d}V}{\mathrm{d}s}\frac{\mathrm{d}s}{\mathrm{d}t} = V'\frac{V}{D} = -\frac{\rho SC_DV^2}{2m}$$

$$\Rightarrow \frac{V'}{V} = \frac{-\rho SDC_D}{2m} = -C_D^* \tag{4}$$

and the four transverse components of motion are reduced to a pair of equations by using complex variables,

$$\tilde{\xi}_B' - \tilde{\xi}_BC_D^* - i\gamma_B\tilde{\mu}_B = \tilde{C}_{NB}^*e^{i\phi_{NB}} + (\tilde{g}_y + i\tilde{g}_z)(D/V^2) + [(\tilde{F}_{Y\mathrm{TB}} + i\tilde{F}_{Z\mathrm{TB}})/m_B](D/V^2) \tag{5a}$$

$$\tilde{\mu}_B' - C_D^*\tilde{\mu}_B - i\sigma_B\iota_B\phi_B'\tilde{\mu}_B = \tilde{C}_{MB}^*e^{i\phi_{MB}}k_{tB}^{-2} + (D^3/V^2)[(\tilde{F}_{Z\mathrm{TB}} - i\tilde{F}_{Y\mathrm{TB}})/I_{yB}]l_{BT} + (D^2/V^2)[(\tilde{M}_Y + i\tilde{M}_Z)/I_{yB}] \tag{5b}$$

For the tail, in a nonrolling coordinate system parallel to that of the body $X''Y''Z''$, at the c.g. (Fig. 1),

$$\tilde{\xi}_T' - \tilde{\xi}_TC_D^* - i\gamma_T\tilde{\mu}_T = \tilde{C}_{NT}^*e^{i\phi_{NT}} + (\tilde{g}_y + i\tilde{g}_z)(D/V^2) - [(\tilde{F}_{Y\mathrm{TB}} + i\tilde{F}_{Z\mathrm{TB}})/m_T](D/V^2) \tag{6a}$$

$$\tilde{\mu}_T' - C_D^*\tilde{\mu}_T - i\sigma_T\iota_T\phi_T'\tilde{\mu}_T = \tilde{C}_{MT}^*e^{i\phi_{MT}}k_{tT}^{-2} - (D^2/V^2)[(\tilde{M}_Y + i\tilde{M}_Z)/I_{yT}] \tag{6b}$$

the actions between the body and tail are equal but with opposite signs. The force exerted by the body on the tail is considered to be applied to the c.g. of the tail.

When a third set of nonrolling axes at the global c.g. of the rocket XYZ is considered, where the velocity is $(u, \tilde{v}, \tilde{w})$, the angular velocity is $(p, \tilde{q}, \tilde{r})$, and the angular velocity of the coordinate system is $(0, \tilde{q}, \tilde{r})$, the following kinematic relationships will hold:

$$\tilde{\mu}_B = \tilde{\mu}_T = \tilde{\mu} \tag{7a}$$

$$(u_B, \tilde{v}_B, \tilde{w}_B) = (u, \tilde{v}, \tilde{w}) + (0, \tilde{q}, \tilde{r}) \wedge l_BD\bar{i} = (u, \tilde{v} + \tilde{r}l_BD, \tilde{w} - \tilde{q}l_BD) \tag{7b}$$

$$(u_T, \tilde{v}_T, \tilde{w}_T) = (u, \tilde{v}, \tilde{w}) + (0, \tilde{q}, \tilde{r}) \wedge (-l_TD)\bar{i} = (u, \tilde{v} - \tilde{r}l_BD, \tilde{w} + \tilde{q}l_BD) \tag{7c}$$

Therefore,

$$u_B = u_T = u \tag{8a}$$

$$\tilde{\xi}_B = (\tilde{v}_B + i\tilde{w}_B)/V = \tilde{\xi} + (\tilde{r}l_BD - i\tilde{q}l_BD)/V = \tilde{\xi} - i\tilde{\mu}l_B \tag{8b}$$

$$\tilde{\xi}_T = (\tilde{v}_T + i\tilde{w}_T)/V = \tilde{\xi} + (-\tilde{r}l_TD + i\tilde{q}l_TD)/V = \tilde{\xi} + i\tilde{\mu}l_T \tag{8c}$$

Relations (8) are substituted in Eqs. (5) and (6), thus, the four-equation system is arrived at:

$$\tilde{\xi}' - i\tilde{\mu}'l_B - C_D^*\tilde{\xi} + C_D^*i\tilde{\mu}l_B - i\gamma\tilde{\mu} = \tilde{C}_{NB}^*e^{i\phi_{NB}} + (\tilde{g}_y + i\tilde{g}_z) \times (D/V^2) + [(\tilde{F}_{Y\mathrm{TB}} + i\tilde{F}_{Z\mathrm{TB}})/m_B](D/V^2) \tag{9}$$

$$\tilde{\mu}' - C_D^*\tilde{\mu} - i\sigma_B\iota_B\phi_B'\tilde{\mu} = \tilde{C}_{MB}^*e^{i\phi_{MB}}k_{tB}^{-2} + (D^3/V^2)[(\tilde{F}_{Z\mathrm{TB}} - i\tilde{F}_{Y\mathrm{TB}})/I_{yB}]l_{BT} + (D^2/V^2)[(\tilde{M}_Y + i\tilde{M}_Z)/I_{yB}] \tag{10}$$

$$\tilde{\xi}' + i\tilde{\mu}'l_T - C_D^*\tilde{\xi} - C_D^*i\tilde{\mu}l_T - i\gamma\tilde{\mu} = \tilde{C}_{NT}^*e^{i\phi_{NT}} + (\tilde{g}_y + i\tilde{g}_z) \times (D/V^2) - [(\tilde{F}_{Y\mathrm{TB}} + i\tilde{F}_{Z\mathrm{TB}})/m_T](D/V^2) \tag{11}$$

$$\tilde{\mu}' - C_D^*\tilde{\mu} - i\sigma_T\iota_T\phi_T'\tilde{\mu} = \tilde{C}_{MT}^*e^{i\phi_{MT}}k_{tT}^{-2} - (D^2/V^2) \times [(\tilde{M}_Y + i\tilde{M}_Z)/I_{yT}] \tag{12}$$

Forces

If Eq. (9) is multiplied by m_B and added to Eq. (11) multiplied by m_T, Eq. (13) is obtained:

$$\tilde{\xi}' - C_D^*\tilde{\xi} - i\gamma\tilde{\mu} = \tilde{C}_N^* e^{i\phi_N} + (\tilde{g}_y + i\tilde{g}_z)(D/V^2) \tag{13}$$

where $\tilde{C}_N^* e^{i\phi_N}$ represents the total aerodynamic force coefficient acting on the configuration and where the equality $m_B l_B D = m_T l_T D$ is introduced.

Moments

The total aerodynamic moment acting on the configuration

$$(\rho SDV^2/2)\tilde{C}_M e^{i\phi_M} = (\rho SDV^2/2)\tilde{C}_{MB} e^{i\phi_{MB}} + (\rho SDV^2/2)\tilde{C}_{MT} e^{i\phi_{MT}} + \left(il_B D\rho SV^2/2\right)\tilde{C}_{NB} e^{i\phi_{NB}} - \left(il_T D\rho SV^2/2\right)\tilde{C}_{NT} e^{i\phi_{NT}} \tag{14}$$

can be obtained by combining Eqs. (9–12), as follows:

$$(\rho SDV^2/2)\tilde{C}_M e^{i\phi_M} = mV^2\tilde{C}_M^* e^{i\phi_M} V^2\left\{\left(I_{yB}/D^2\right)\langle\langle(10)\rangle\rangle + \left(I_{yT}/D^2\right)\langle\langle(12)\rangle\rangle + m_B i l_B\langle\langle(9)\rangle\rangle - m_T i l_T\langle\langle(11)\rangle\rangle\right\} \tag{15}$$

By substitution of the terms shown, and by the introduction of $I_y = I_{yB} + I_{yT} + m_B l_B^2 D^2 + m_T l_T^2 D^2$,

$$\tilde{\mu}' - C_D^*\tilde{\mu} - i\tilde{\mu}(\sigma_B\phi_B' + \sigma_T\phi_T') = \tilde{C}_M^* e^{i\phi_M} k_t^{-2} \tag{16}$$

Equations (13) and (16) describe the lateral motion of a free-rolling tail configuration. The differences with respect to the equations describing the lateral motion of a fixed-tail rocket[5] arise from the existence of two different roll rates.

Linearization of Forces and Moments

Forces

The term representing the total aerodynamic force coefficient acting on the configuration $\tilde{C}_N^* e^{i\phi_N}$ of Eq. (13) is

$$(\rho SD/2m)\tilde{C}_N e^{i\phi_N} = (\rho SD/2m)\left[\tilde{C}_{NB} e^{i\phi_{NB}} + \tilde{C}_{NT} e^{i\phi_{NT}}\right] \tag{17}$$

In the nonrolling body c.g. centered-fixed system, the body force coefficient can be linearized as follows[5]:

$$\tilde{C}_{NB} e^{i\phi_{NB}} = -[C_{\hat{N}B\alpha} + i\phi_B' C_{\hat{N}Bp\alpha}]\tilde{\xi}_B - [\phi_B' C_{\hat{N}Bpq} + iC_{\hat{N}Bq}]\tilde{\mu}_B - [C_{\hat{N}B\dot{\alpha}} + i\phi_B' C_{\hat{N}Bp\dot{\alpha}}][\tilde{\xi}_B' + i\phi_B'\tilde{\xi}_B] - [\phi_B' C_{\hat{N}Bp\dot{q}} + iC_{\hat{N}B\dot{q}}] \times [\tilde{\mu}_B' + i\phi_B'\tilde{\mu}_B] \tag{18}$$

where the tilde superscripts denote aerodynamic coefficients in the body c.g. centered nonrolling system. If the kinematic relations (8) are substituted into this expression, the change in aerodynamic coefficients when expressed with respect to the global c.g. is taken into consideration, and all coefficients without a measurable effect are omitted,[5] then Eq. (18) takes the final form

$$\tilde{C}_{NB} e^{i\phi_{NB}} = -[C_{NB\alpha} + i\phi_B' C_{NBp\alpha}]\tilde{\xi} - iC_{NBq}\tilde{\mu} - C_{NB\dot{\alpha}}\tilde{\xi}' \tag{19}$$

Likewise, the tail force coefficient can be expressed as

$$\tilde{C}_{NT} e^{i\phi_{NT}} = -[C_{NT\alpha} + i\phi_T' C_{NTp\alpha}]\tilde{\xi} - iC_{NTq}\tilde{\mu} - C_{NT\dot{\alpha}}\tilde{\xi}' \tag{20}$$

Therefore, the total aerodynamic force coefficient acting on the configuration is

$$\tilde{C}_N e^{i\phi_N} = -[C_{N\alpha} + i\phi_B' C_{NBp\alpha} + i\phi_T' C_{NTp\alpha}]\tilde{\xi} - iC_{Nq}\tilde{\mu} - C_{N\dot{\alpha}}\tilde{\xi}' \tag{21}$$

where

$$C_{NB\alpha} + C_{NT\alpha} = C_{N\alpha} \tag{22a}$$

$$C_{NB\dot{\alpha}} + C_{NT\dot{\alpha}} = C_{N\dot{\alpha}} \tag{22b}$$

$$C_{NBq} + C_{NTq} = C_{Nq} \tag{22c}$$

Moments

The total aerodynamic moment acting on the configuration is

$$\tilde{C}_M e^{i\phi_M} = \tilde{C}_{MB} e^{i\phi_{MB}} + \tilde{C}_{MT} e^{i\phi_{MT}} + il_B\tilde{C}_{NB} e^{i\phi_{NB}} - il_T\tilde{C}_{NT} e^{i\phi_{NT}} \tag{23}$$

By repetition of the derivation used with forces, Eq. (23) becomes

$$\tilde{C}_M e^{i\phi_M} = [\phi_B' C_{mBp\alpha} + \phi_T' C_{mTp\alpha} + l_B\phi_B' C_{NBp\alpha} - l_T\phi_T' C_{NTp\alpha} - iC_{m\alpha}]\tilde{\xi} + C_{mq}\tilde{\mu} - iC_{m\dot{\alpha}}\tilde{\xi}' \tag{24}$$

where

$$C_{mB\alpha} + C_{mT\alpha} + l_B C_{NB\alpha} - l_T C_{NT\alpha} = C_{m\alpha} \tag{25a}$$

$$C_{mBq} + C_{mTq} + l_B C_{NBq} - l_T C_{NTq} = C_{mq} \tag{25b}$$

$$C_{mB\dot{\alpha}} + C_{mT\dot{\alpha}} + l_B C_{NB\dot{\alpha}} - l_T C_{NT\dot{\alpha}} = C_{m\dot{\alpha}} \tag{25c}$$

The differences between linearized expressions for force and moment coefficients compared to those for a fixed-tail rocket[5] arise once again from the existence of two roll rates.

Differential Equation of Motion

If Eqs. (21) and (24) are substituted into Eqs. (13) and (16), and μ, and μ' are eliminated, the linear differential equation of motion will be

$$\tilde{\xi}'' + A_1\tilde{\xi}' - A_2\tilde{\xi} = A_3 \tag{26}$$

where the coefficients are

$$A_1 = C_{L\alpha}^* - C_D^* - k_t^{-2}\left(C_{mq}^* + C_{m\dot{\alpha}}^*\right) - i(\sigma_B\phi_B' + \sigma_T\phi_T') \tag{27}$$

$$A_2 = k_t^{-2}C_{m\alpha}^* + i(\sigma_B\phi_B' + \sigma_T\phi_T')C_{L\alpha}^* + ik_t^{-2}(\rho SD/2m)[\phi_B' C_{mBp\alpha} + \phi_T' C_{mTp\alpha} + l_B\phi_B' C_{NBp\alpha} - l_T\phi_T' C_{NTp\alpha}] \tag{28}$$

$$A_3 = (\sigma_B\phi_B' + \sigma_T\phi_T')(gD/V^2) \tag{29}$$

where a flat trajectory was assumed, arc length derivatives of the lift and Magnus force coefficients were omitted (see Ref. 5) and the approximation $C_{N\alpha}^* - C_D^* \approx C_{L\alpha}^*$ was introduced.

Equivalent gyroscopic and Magnus roll rates p_g and p_m are introduced:

$$\sigma\phi_g' = \sigma_B\phi_B' + \sigma_T\phi_T' \tag{30}$$

$$\phi_m' C_{mp\alpha} = \phi_B' C_{mBp\alpha} + \phi_T' C_{mTp\alpha} + l_B\phi_B' C_{NBp\alpha} - l_T\phi_T' C_{NTp\alpha} \tag{31}$$

where $C_{mp\alpha}$ is the Magnus moment coefficient derivative of the configuration with the tail fixed and $\phi_m'$is the roll rate, giving a Magnus moment equal to the Magnus moment of the free-rolling tail rocket.

Now, a modified Magnus moment coefficient derivative is considered:

$$C_{\hat{m}p\alpha} = C_{mp\alpha}(p_m/p_g) = C_{mp\alpha}(\phi_m'/\phi_g') \tag{32}$$

where, for a given configuration, the ratio ϕ_m'/ϕ_g' is assumed to be independent of roll rates.

In terms of the definitions (30–32), the coefficients of the linear equation of motion (26) are

$$A_1 = C_{L\alpha}^* - C_D^* - k_t^{-2}\left(C_{mq}^* + C_{m\dot{\alpha}}^*\right) - i\sigma\phi_g' \tag{33}$$

$$A_2 = k_t^{-2}C_{m\alpha}^* + i\sigma\phi_g'\left(C_{L\alpha}^* + k_a^{-2}C_{\hat{m}p\alpha}^*\right) \tag{34}$$

$$A_3 = \sigma\phi_g'(gD/V^2) \tag{35}$$

The resulting differential equation (26) describes the lateral motion of a symmetric fixed-tail rocket with a roll rate ϕ_g' given by Eq. (30) and a modified Magnus moment coefficient derivative $C_{\hat{m}p\alpha}$ given by Eq. (32).

Magnus Effects on Free-Rolling Tail Missiles

By the use of Eq. (30), the determination of the gyroscopic equivalent roll rate ϕ'_g at any trajectory point for given body and tail roll rates is straightforward. However, the equivalent Magnus rate ϕ'_m or the $C_{\hat{m}p\alpha}$ value to be introduced into Eq. (26) is not very clear.

In a missile employing canted fins to produce the roll rotational speed to reduce dispersion, a free-rolling tail will attain considerably higher p_T rates than the whole configuration with the tail fixed p_F. The body spin p_B will keep well below the fixed-tail configuration rate p_F because it is accelerated only by the deliberately small body-tail bearing friction. If Magnus effects were mainly the result of the body spin, free-rolling tail configurations would be comparatively free from these effects because of lower body roll rates. Unfortunately, this is not so. There are additional sources of Magnus force and moment due to body–tail interference, leading-edge suction, and fin cant (see Refs. 6 and 7).

Wind-tunnel and flight testing of free-rolling tail configurations[4] show that the Magnus force and moment are nearly identical for both the fixed and the free-rolling tail for a given configuration at small angles of attack when the fin cant angle is kept constant. At higher angles of attack, Magnus moments are smaller for free-rolling tail configurations. No matter what means of producing roll rotational speeds is used, according to these results, it may be advisable to assume parity between Magnus effects for the free-rolling tail and the fixed-tail rocket at low angles of attack:

$$\phi'_B C_{mBp\alpha} + \phi'_T C_{mTp\alpha} + l_B \phi'_B C_{NBp\alpha} - l_T \phi'_T C_{NTp\alpha}$$

$$= \phi'_m C_{mp\alpha} \approx \phi'_F C_{mp\alpha} \approx \phi'_g C_{mp\alpha} \tag{36}$$

The last equality is based on the assumption that p_g is a good approximation of the fixed-tail configuration rate p_F, provided that the damping in roll is not too large.

By the introduction of Eq. (32) into Eq. (36),

$$C_{\hat{m}p\alpha} \approx C_{mp\alpha}$$

At higher angles of attack

$$\phi'_m C_{mp\alpha} \prec \phi'_F C_{mp\alpha} \approx \phi'_g C_{mp\alpha} \tag{37}$$

By the introduction of Eq. (32) into Eq. (37),

$$C_{\hat{m}p\alpha} \prec C_{mp\alpha}$$

Effect of Asymmetries

The effect of aerodynamic and inertial asymmetries can be considered by introducing constant normal forces and moments when the angle of attack is zero. The body asymmetry is a forcing function of frequency $p_B$in the nonrolling axis system, whereas the tail asymmetry is a forcing function of frequency p_T. With temporary disregard for the gravity term given by Eq. (35), the differential equation of motion would be

$$\tilde{\xi}'' + A_1 \tilde{\xi}' - A_2 \tilde{\xi} = -F_B e^{i\phi_B} - F_T e^{i\phi_T} \tag{38}$$

where

$$F_B = \left(\rho S D^3 / 2I_y\right)\left[C_{MB0} e^{i\phi_{MB0}} - i k_t^2 (\phi'_B - \sigma \phi'_g) C_{NB0} e^{i\phi_{NB0}}\right] \tag{39}$$

$$F_T = \left(\rho S D^3 / 2I_y\right)\left[C_{MT0} e^{i\phi_{MT0}} - i k_t^2 (\phi'_T - \sigma \phi'_g) C_{NT0} e^{i\phi_{NT0}}\right] \tag{40}$$

The particular solutions for these forcing functions take the form $\tilde{\xi}_B = \xi_B e^{i\phi_B}$ and $\tilde{\xi}_T = \xi_T e^{i\phi_T}$.

By substitution of the particular solutions in Eq. (38), the following expressions for the constants are obtained:

$$\xi_B = F_B \Big/ \left(\phi'^2_B - A_1 i \phi'_B + A_2\right) \tag{41}$$

$$\xi_T = F_T \Big/ \left(\phi'^2_T - A_1 i \phi'_T + A_2\right) \tag{42}$$

Equivalent Fixed-Tail Rocket

For a given slightly unsymmetrical free-rolling tail rocket, a dynamically equivalent fixed-tail configuration can be defined by introducing the equivalent gyroscopic roll rate ϕ'_g of Eq. (30) and the modified Magnus moment coefficient derivative $C_{\hat{m}p\alpha}$ of Eq. (32). The differential equation of motion will be

$$\tilde{\xi}'' + A_1 \tilde{\xi}' - A_2 \tilde{\xi} = A_3 - F_B e^{i\phi_B} - F_T e^{i\phi_T} \tag{43}$$

where the coefficients A_1, A_2, A_3, F_B, and F_T are given by Eqs. (33), (34), (35), (39), and (40), respectively. For steady-state conditions, the general solution of Eq. (43) is

$$\tilde{\xi} = \tilde{\xi}_g + K_1 e^{i\phi_1} + K_2 e^{i\phi_2} + \xi_B e^{i\phi_B} + \xi_T e^{i\phi_T} \tag{44}$$

where

$$\tilde{\xi}_g = A_3/A_2, \qquad K_j = K_{j0} e^{\lambda_j s}, \qquad \phi_j = \phi_{j0} + \phi'_j s$$

$$\lambda_j + i\phi'_j = (1/2)\left[-A_1 \pm \sqrt{A_1^2 + 4A_2}\right] \tag{45}$$

and ξ_B and ξ_T are given by Eqs. (41) and (42).

Resonance

With disregard for gravity effects, the last two terms in Eq. (44) can be considered the steady-state trim angles corresponding to body and tail asymmetries, when the modal waves have damped to negligible magnitudes:

$$\tilde{\xi} = \xi_B e^{i\phi_B} + \xi_T e^{i\phi_T} \tag{46}$$

These trim angles are body and tail fixed,[8] and, accordingly, they rotate at p_B and p_T, respectively, in nonrolling axes as shown in Fig. 2. In body- and tail-fixed axes, their magnitude and orientation are given by Eqs. (41) and (42), respectively:

$$\xi_B = F_B \Big/ \left(\phi'^2_B - A_1 i \phi'_B + A_2\right) = F_B/(\mathrm{Re}_B - i\,\mathrm{Im}_B) \tag{47}$$

$$\xi_T = F_T \Big/ \left(\phi'^2_T - A_1 i \phi'_T + A_2\right) = F_T/(\mathrm{Re}_T - i\,\mathrm{Im}_T) \tag{48}$$

where $\mathrm{Re}_{B,T}$ and $\mathrm{Im}_{B,T}$ are the real and imaginary parts of the denominators. By the introduction of Eqs. (33), (34), and (30) in Eqs. (47) and (48)

$$\mathrm{Re}_B = \phi'^2_B (1 - \sigma_B) - \sigma_T \phi'_T \phi'_B + M \tag{49a}$$

$$\mathrm{Im}_B = \phi'_B (H - \sigma_B T) - \sigma_T \phi'_T T \tag{49b}$$

$$\mathrm{Re}_T = \phi'^2_T (1 - \sigma_T) - \sigma_B \phi'_B \phi'_T + M \tag{50a}$$

$$\mathrm{Im}_T = \phi'_T (H - \sigma_T T) - \sigma_B \phi'_B T \tag{50b}$$

where

$$H = C^*_{L\alpha} - C^*_D - k_t^{-2}\left(C^*_{mq} + C^*_{m\dot{\alpha}}\right) \tag{51a}$$

$$T = C^*_{L\alpha} + k_a^{-2} C^*_{\hat{m}p\alpha} \tag{51b}$$

$$M = k_t^{-2} C^*_{m\alpha} \tag{51c}$$

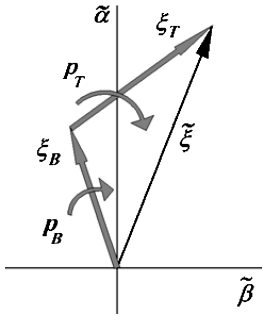

Fig. 2 Body and tail trim angles.

Focusing on the tail term of Eq. (48), if Re_T becomes zero at any trajectory point, the familiar situation of linear resonance[8] occurs, characterized by high trim amplitudes and a −90-deg phase shift with respect to the zero roll rate trim angle orientation. Re_T is zero when

$$\phi'_T = \phi'_{Tr} = \frac{\sigma_B \phi'_B}{2(1-\sigma_T)} + \sqrt{\frac{\sigma_B^2 \phi_B'^2}{4(1-\sigma_T)^2} - \frac{M}{(1-\sigma_T)}} \tag{52}$$

The resonance frequency increases almost linearly with the $\sigma_B \phi'_B$ term, compared to the fixed tail case where the crossover frequency is

$$\phi'_{Fr} = \sqrt{-M/(1-\sigma)} \approx \sqrt{-M} \tag{53}$$

For realistic inertial and body rate figures, Eq. (52) gives a frequency of resonance that is only 1–2% higher than the value for zero body spin, even in dealing with inertially low slender configurations and high body rates. Thus, for practical purposes, the resonance still takes place when the tail rate matches the zero spin pitch frequency:

$$\phi'_{Tr} \approx \sqrt{-M/(1-\sigma_T)} \approx \sqrt{-M} \tag{54}$$

An identical derivation and remarks can be made concerning the body term given by Eq. (47):

$$\phi'_{Br} = \frac{\sigma_T \phi'_T}{2(1-\sigma_B)} + \sqrt{\frac{\sigma_T^2 \phi_T'^2}{4(1-\sigma_B)^2} - \frac{M}{(1-\sigma_B)}} \approx \sqrt{-M} \tag{55}$$

In body- and tail-fixed axes, respectively, the resonant trim angles are

$$\xi_{Br} = F_B/-i\mathrm{Im}_B = F_B/-i[\phi'_{Br}(H-\sigma_B T) - \sigma_T \phi'_T T] \tag{56a}$$

$$\xi_{Tr} = F_T/-i\mathrm{Im}_T = F_T/-i[\phi'_{Tr}(H-\sigma_T T) - \sigma_B \phi'_B T] \tag{56b}$$

The changes in T due to reduced Magnus moments at the high resonant trim angles ($C_{\hat{m}p\alpha} \prec C_{mp\alpha}$), are considerably lessened by T being multiplied by $\sigma_{B,T}$.

The presence of cross terms in Eqs. (52), (55), and (56) do not significantly alter the resonance frequencies or the trim angles resulting from the values for zero body or tail spin. Figure 3 shows the total trim angles in a case where the static trim angles (zero spin), corresponding to body and tail asymmetries, are both 0.5 deg. The influence of body or tail roll rates on the peak resonant trim tail or body angles is negligible.

Even though they are very weakly coupled, body and tail trim angles act jointly. Figure 4 shows the total body trim angle and a vertical plane passing through the peak trim tail line.

Under the assumption that the tail is at resonance $\phi'_T = \phi'_{Tr} \approx \sqrt{-M}$, the contribution of the body trim angle is not negligible for body rates close to the resonant value, $\phi'_{Br} \approx -M$, near or at the point indicated by the arrow. Figure 5 shows the situation as seen from the tail-fixed axes system.

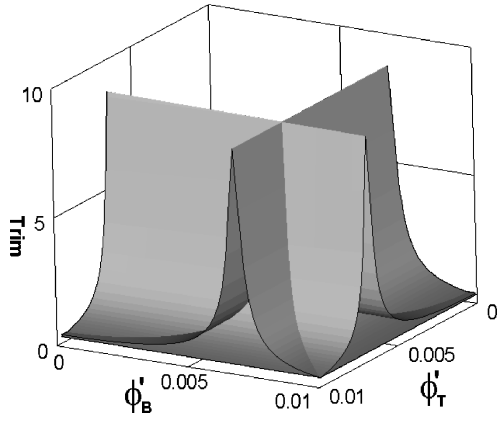

Fig. 3 Body and tail trim angles.

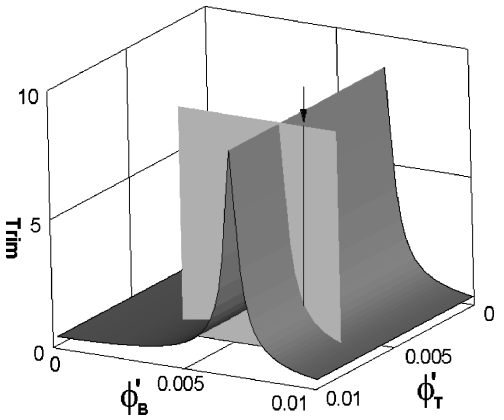

Fig. 4 Body trim angle and tail trace plane.

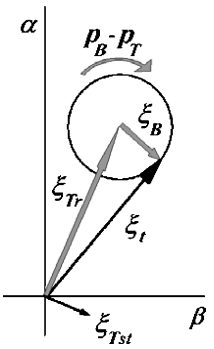

Fig. 5 Trim angle in tail-fixed axes.

The resulting complex angle of attack is the sum of a fixed component ξ_{Tr} that is due to the resonant tail trim angle and a rotating component ξ_B, which is in turn due to the body trim angle. Note that ξ_{Tr} is the result of the amplification and the shift of −90-deg of the static tail trim value ξ_{Tst}. The rate of the ξ_B component equals the difference between body and tail rates. For positive spin rates, ξ_B rotates counterclockwise if $p_{Tr} > p_B$, and clockwise if $p_B > p_{Tr}$. If the difference between p_B and p_{Tr} decreases, ξ_B increases up to the resonance value when $p_B = p_{Br} = p_{Tr}$. At this point, the configuration has turned into a fixed-tail rocket.

Resonance Lock-In

Linear resonance caused by small asymmetries does not justify the destructive behavior sometimes shown by unguided rockets rolling near the pitch frequency.[9,10] Because of the continuously changing environment, the passage through resonance should only slightly affect the angular motion of the missile. The contribution of nonlinear induced roll moments, due to trim angles caused by aerodynamic[11] and inertial[12] asymmetries, may push the missile into a state of sustained resonance where induced roll moments cancel the roll commanded by the deliberated fin cant. This so-called lock-in condition is accompanied by pitch–yaw motions varying from slight disturbances to the large angular amplitudes (catastrophic yaw)[11] due to highly nonlinear pitch and yaw moments or to a decreased damping in yaw.[13] The resonance lock-in condition is nonlinear in nature, and it is characterized by a strong degree of coupling among the pitch, yaw, and roll channels.

A nonlinear dynamic model of sustained resonance that preserves lateral motion linearity is feasible,[14] because it allows nonlinear induced moments to be present in the roll channel. The assumption of lateral motion linearity implies that any roll position-dependent component of the transverse force or moment is neglected. The model precludes the forecast of catastrophic yaw unless this is considered to be the result of a decrease of the yaw damping level.[13]

According to this model, the steady-state lateral response to the aerodynamic trim takes the form of Eq. (46):

$$\tilde{\xi} = \xi_B e^{i\phi_B} + \xi_T e^{i\phi_T} \tag{57}$$

and the time-dependent roll equation for the tail is

$$I_{xT}\dot{p}_T = q_d SD[Cl_{\delta T}\delta + Cl_{pT}(p_T D/V) + Cl_{iT}] - \kappa(p_T - p_B) \tag{58}$$

where a nonlinear induced roll moment coefficient and the bearing friction moment were included.

By the use of dimensionless distance s as an independent variable again,

$$\phi_T' = p_T D/V, \qquad \phi_T'' = (D/V)^2\left[\dot{p}_T + (V/D)C_D^* p_T\right]$$

After a few derivations, Eq. (58) becomes

$$\phi_T'' + \phi_T'(K_{pT} + V_{fT}/V) - (V_{fT}/V)\phi_B' - K_\delta - K_{iT} = 0 \tag{59}$$

where

$$K_{pT} = -\left(C_D^* + k_{aT}^{-2}Cl_{pT}^*\right) \tag{60a}$$

$$K_\delta = k_{aT}^{-2}Cl_{\delta T}^*\delta \tag{60b}$$

$$V_{fT} = k_{aT}^{-2}(\kappa/m_T D) \tag{60c}$$

$$K_{iT} = k_{aT}^{-2}Cl_{iT}^* \tag{60d}$$

Similarly, the body roll equation becomes

$$\phi_B'' + \phi_B'[K_{pB} + (V_{fB}/V)] - (V_{fB}/V)\phi_T' - K_{iB} = 0 \tag{61}$$

where definitions (60) still apply by simply changing the subscript T to B.

Nonlinear induced roll moments Cl_{iB} and Cl_{iT} are due to angles of attack originated by configurational asymmetries and c.m. offsets. They augment with the total angle of attack and vary with the orientation of the angle-of-attack plane with respect to body- and tail-fixed axes $\theta_{B,T}$. For a configuration possessing n-gonal symmetry, where n is the number of covering operations[15] resulting from its rotational symmetry, the induced roll moment may be expressed by a Fourier sine series in θ. By retention of the first term in this series, in terms of the angle of attack in fixed axes, the induced roll moment is

$$Cl_{iB,T} = -iC_{B,T}\left(\xi_{b,t}^n - \bar{\xi}_{b,t}^n\right)/2 \tag{62}$$

In a symmetric body with a laterally offset mass center, the induced roll moment takes the form of Eq. (62) for $n=1$ and $C_B = \hat{r}C_{N\alpha}$ (Refs. 10 and 14). A cruciform tail has an induced roll moment, taking the form of Eq. (62) for $n=4$. Figure 6 shows the induced roll moment for a cruciform tail at $\theta_T = 22.5$ deg.

The moment is usually negative at small angles of attack,[9] becoming positive for angles greater than a certain value ($\alpha^* \approx 15$ deg).

Note that $\xi_{b,t}$ is the total angle of attack as seen from the body and the tail, respectively:

$$\xi_b = \xi_B + \xi_T e^{i(\phi_T - \phi_B)} \tag{63}$$

$$\xi_t = \xi_T + \xi_B e^{i(\phi_B - \phi_T)} \tag{64}$$

The total angle of attack, from Eq. (63) or Eq. (64), is the sum of a fixed component $\xi_{B,T}$ and a rotary component spinning at the difference between body and tail roll rates. Under the assumption that body and tail rates are considerably differentiated, the rate of the spinning components is large, and the induced roll moments may be assumed to be the result of the average values of Eqs. (63) and (64), ξ_B and ξ_T.

Therefore,

$$Cl_{iB,T} = -iC_{B,T}\left(\xi_{b,t}^n - \bar{\xi}_{b,t}^n\right)/2 \approx -iC_{B,T}\left(\xi_{B,T}^n - \bar{\xi}_{B,T}^n\right)/2 \tag{65}$$

For a body of revolution with a mass center offset,

$$K_{iB} = \frac{-i}{2}k_{aB}^{-2}\hat{r}C_{N\alpha}^*\frac{m}{m_B}(\xi_B - \bar{\xi}_B)$$

$$= \frac{k_{aB}^{-2}\hat{r}C_{N\alpha}^* k_t^{-2}C_{MB0}^*(\cos\phi_{MB0}\mathrm{Im}_B + \sin\phi_{MB0}\mathrm{Re}_B)}{\mathrm{Re}_B^2 + \mathrm{Im}_B^2} \tag{66}$$

where the CN_{B0} term describing the forcing function for the body of Eq. (39) was ignored,

$$F_B = (\rho SD^3/2I_y)C_{MB0}e^{i\phi_{MB0}} = k_t^{-2}C_{MB0}^*(m_B/m)e^{i\phi_{MB0}} \tag{67}$$

For a cruciform tail,

$$K_{iT} = \frac{-i}{2}k_{aT}^{-2}C_T^*\left(\xi_T^4 - \bar{\xi}_T^4\right) = \frac{k_{aT}^{-2}C_T^*\left|F_T\right|^4}{[\mathrm{Re}_T^2 + \mathrm{Im}_T^2]^4}\left\{4\cos 4\phi_{MT0}\left(\mathrm{Re}_T^2\right.\right.$$

$$\left.\left. - \mathrm{Im}_T^2\right)\mathrm{Re}_T\mathrm{Im}_T + \sin 4\phi_{MT0}\left(\mathrm{Re}_T^4 + \mathrm{Im}_T^4 - 6\mathrm{Re}_T^2\mathrm{Im}_T^2\right)\right\} \tag{68}$$

where the C_{NT0} term of the forcing function for the tail of Eq. (40) was ignored,

$$F_T = \left(\rho SD^3/2I_y\right)C_{MT0}e^{i\phi_{MT0}} = k_t^{-2}C_{MT0}^*(m_T/m)e^{i\phi_{MT0}}$$

$$= |F_T|e^{i\phi_{MT0}} \tag{69}$$

Equations (47), (48), (57), (59), and (61) and expressions (49), (50), (60), (66), and (68) describe the dynamics of the system. Sustained resonance occurs when Eq. (59) or Eq. (61) has a constant steady-state solution near the resonance frequency $\phi_{Tr}' \approx \sqrt{-M}$ or $\phi_{Br}' \approx \sqrt{-M}$, respectively. No simultaneous occurrence of both solutions is considered here because this would correspond to the fixed-tail case.

Steady-state solutions of Eqs. (59) and (61) can be interpreted graphically. If ϕ_B' attains a steady-state value ($\phi_B'' = 0$), Eq. (61) is equivalent to finding the intersection between a plane $\pi(\phi_B', \phi_T')$ and the surface $K_{iB}(\phi_B', \phi_T')$:

$$\phi_B'[K_{pB} + V_{fB}/V] - (V_{fB}/V)\phi_T' = K_{iB} \tag{70}$$

To illustrate the dynamics of the system, a special case is considered. For the particular arrangement of body asymmetries shown in Fig. 7, the initially ($p_B = 0$) induced roll moment is zero because the static normal force N_{st} is aligned with the c.m.

With increasing p_B, the trim angle shifts counterclockwise, growing to the peak value at resonance, where the associated normal force N_r yields the maximum positive roll moment. For this particular case, the intersection given by Eq. (70) between the plane and the surface when the frictional term (V_{fB}/V) is neglected is shown in

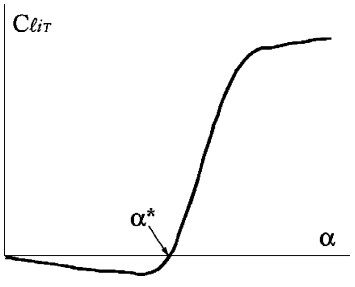

Fig. 6 Tail-induced roll moment.

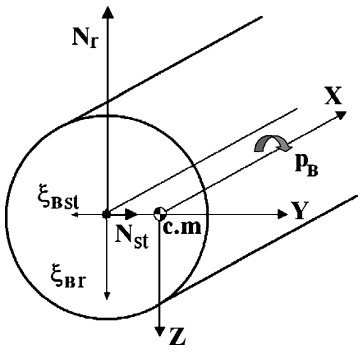

Fig. 7 Laterally offset c.m. and trim response.

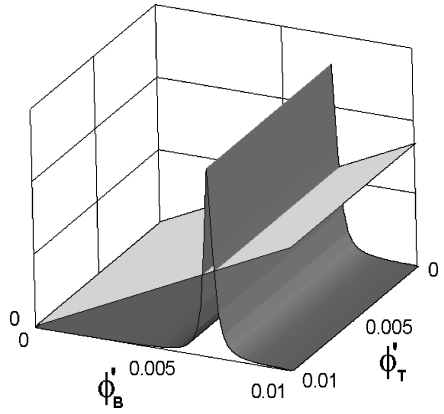

Fig. 8 Plane and induced roll moment without friction.

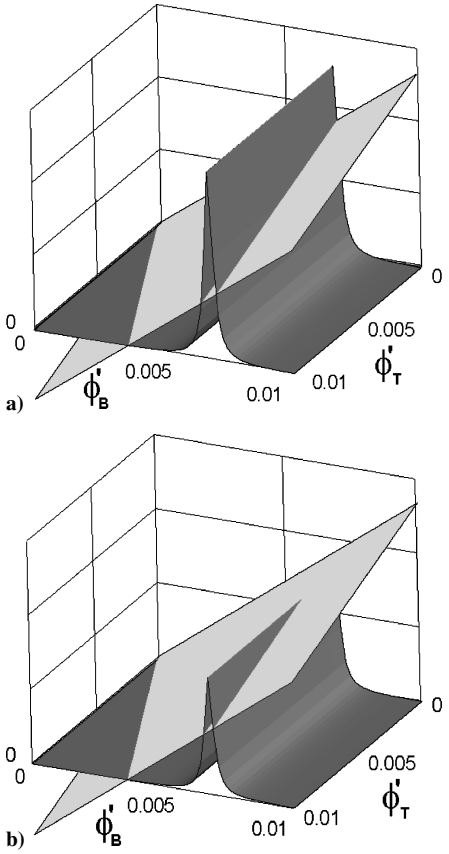

Fig. 9 Plane and induced roll moment with friction.

Fig. 8. The intersections of π and K_{iB} give two types of stable solutions, $\phi'_{Be} = 0 \,\forall\, \phi'_T$ and $\phi'_{Be} \geq \phi'_{Br} \,\forall\, \phi'_T$ for initial body rates below and above ϕ'_{Br}, respectively. Again, the presence of cross terms (ϕ'_T) in K_{iB} do not significantly alter the bidimensionality of the induced roll surface.

Figures 9a and 9b depict the effect of tail–body friction in two different static body trim angles. Steady-state solutions for nonnegligible bearing friction are not ϕ'_T independent.

The body roll acceleration for the case of Fig. 9b, $\phi''_B = K_{iB}(\phi'_B, \phi'_T) - \pi(\phi'_B, \phi'_T)$, is shown in Fig. 10a. The behavior of the system can be described on the planform view shown in Fig. 10b.

Under the assumption that the tail lacks configurational asymmetries ($F_T = 0$), the trim angle, as seen from the tail in Eq. (64), is reduced to the spinning component $\xi_t = \xi_B e^{i(\phi_B - \phi_T)}$. The average tail-induced roll moment and K_{iT} are zero. Steady-state solutions of Eq. (59) are then on a straight line of the following equation:

$$\phi'_{Te} = \frac{K_\delta + (V_{fT}/V)\phi'_{Be}}{K_{pT} + V_{fT}/V} \tag{71}$$

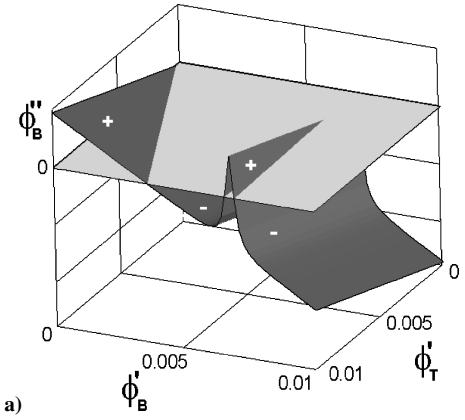

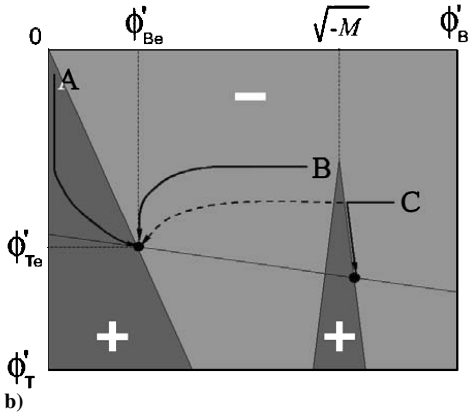

Fig. 10 Body roll acceleration zones.

A free-rolling tail configuration departing from point A will follow a trajectory (ϕ'_B, ϕ'_T) similar to that indicated by the arrow. The fin cant accelerates the tail arrangement quickly at the beginning and the body rate increases, driven by the bearing friction torque. The steady-state rate ϕ'_{Be} is achieved at a point on the borderline ($\phi''_B = 0$) where the driving torque equals the body damping in roll [$\pi(\phi'_B, \phi'_T) = 0$]. At this line, K_{iB} (Fig. 9b) is negligible and Eq. (70) is reduced to the borderline,

$$K_{pB}\phi'_{Be} = (V_{fB}/V)(\phi'_{Te} - \phi'_{Be}) \tag{72}$$

The intersection of the lines given by Eqs. (71) and (72) determines the specific borderline point at which steady-state conditions (ϕ'_{Be}, ϕ'_{Te}) are attained.

If the configuration departs from point B, for example, by spinning the body with a fluted nozzle, a similar comportment is shown, arriving at the steady-state condition (ϕ'_{Be}, ϕ'_{Te}). When departing from point C, the configuration attempts to attain the steady-state solution given by the intersection of lines [Eqs. (71) and (72)], following the dotted arrow in Fig. 10b. When touching the line of zero body roll acceleration due to the induced roll moment, body lock-in occurs at $\phi'_B \approx \phi'_{Br} \approx \sqrt{-M}$. From this point, the tail rate increases up to the equilibrium value on the steady-state solution line given by Eq. (71):

$$\phi'_{Te} \approx \frac{K_\delta + (V_{fT}/V)\sqrt{-M}}{K_{pT} + V_{fT}/V} \tag{73}$$

The bearing friction moment couples the body and tail roll channels and may affect the onset of lock-in conditions depending on the initial conditions. For the case shown in Fig. 9a, the induced roll moment surface does not allow passage of configurations departing from points where $\phi'_B \succ \phi'_{Br}$. As before, when touching the line of intersection between the plane and the induced roll moment surface, body lock-in occurs at $\phi'_B \approx \phi'_{Br} \approx \sqrt{-M}$, and again the tail rate moves to the equilibrium value given by Eq. (73) (not represented). For the case shown in Fig. 8, the channels are completely uncoupled,

and the tail attains the zero friction equilibrium rate:

$$\phi'_{Te} = \frac{K_\delta}{K_{pT}} \tag{74}$$

In the absence of bearing friction, possible interference between channels affecting lock-in conditions can also occur in the case outlined in the preceding section.

If the body is at lock-in, and the tail rate is near the resonance value, the slowly spinning contribution of a trim tail angle ($F_T \neq 0$) in Eq. (63) cannot be ignored. The significant periodic fluctuations of the body trim angle around the average value ξ_{Br} give raise to corresponding low-frequency fluctuations of the body-induced roll surface, thus altering body lock-in conditions. The specific situation presented to show the behavior of the system is not the usual one. For most revolving shells and bodies, K_{pB} is negative because $k_{aB}^{-2} Cl^*_{pB} \prec 0$ is only one-third the size of C^*_D. (On the other hand, K_{pT} is usually positive.[5,14]) The plane then has a negative slope, as shown in Fig. 11a. For the particular arrangement of asymmetries of Fig. 7, reproduced in the upper part of Fig. 11a, no lock-in condition can take place. The single steady-state solution is then the line $\phi'_{Be} = 0 \,\forall\, \phi'_T$.

By the limitation of all possible body configurational asymmetries to lateral c.m. offsets, the body trim pitch moment is caused by the drag force[14] with the lever arm $\hat{r}$. The associated static normal force N_{st} is aligned with the c.m. in the direction opposite to the Y-axis, causing a permanent negative roll moment as shifting occurs. Under these circumstances, lock-in conditions are again possible (Fig. 11b).

The fact that K_{pB} is usually negative can be questioned if the curvature of the trajectory is introduced. (This consideration entails an additional inconsistency in the model because, to preserve lateral motion linearity, a flat trajectory is assumed.) In this case, Eq. (4) presents an additional term due to gravity: $(V'/V) = -C^*_D - g \sin\Theta (D/V^2)$, where Θ is the trajectory angle, and the expression for K_{pB} given by Eqs. (60) becomes

$$K_{pB} = -\left(C^*_D + k_{aB}^{-2} Cl^*_{pB} + g \sin\Theta D \Big/ V^2\right) \tag{75}$$

On the descending limb of the trajectory, Θ is negative; therefore, positive values of K_{pB} can be attained. Under the assumption that lateral c.m. offsets are the only normal body configuration asymmetries, the associated negative roll moments prevent body lock-in conditions from developing, provided that K_{pB} is positive (Fig. 12).

If body lock-in is excluded, the chance of sustained resonance is greatly reduced because large angles of attack are required[10] to cause sufficient tail-induced roll moment (Fig. 6) for tail lock-in occurrence. A similar derivation can be made regarding tail lock-in conditions. The modulation derived from its four-gonal symmetry

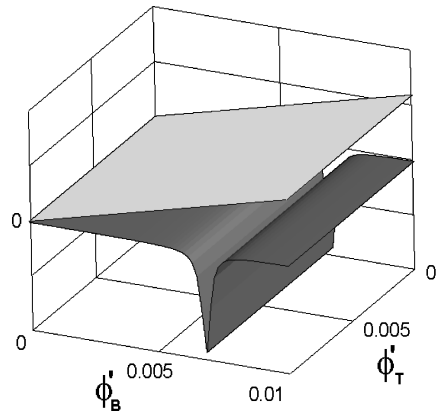

Fig. 12 Plane and induced roll moment for positive K_{pB}.

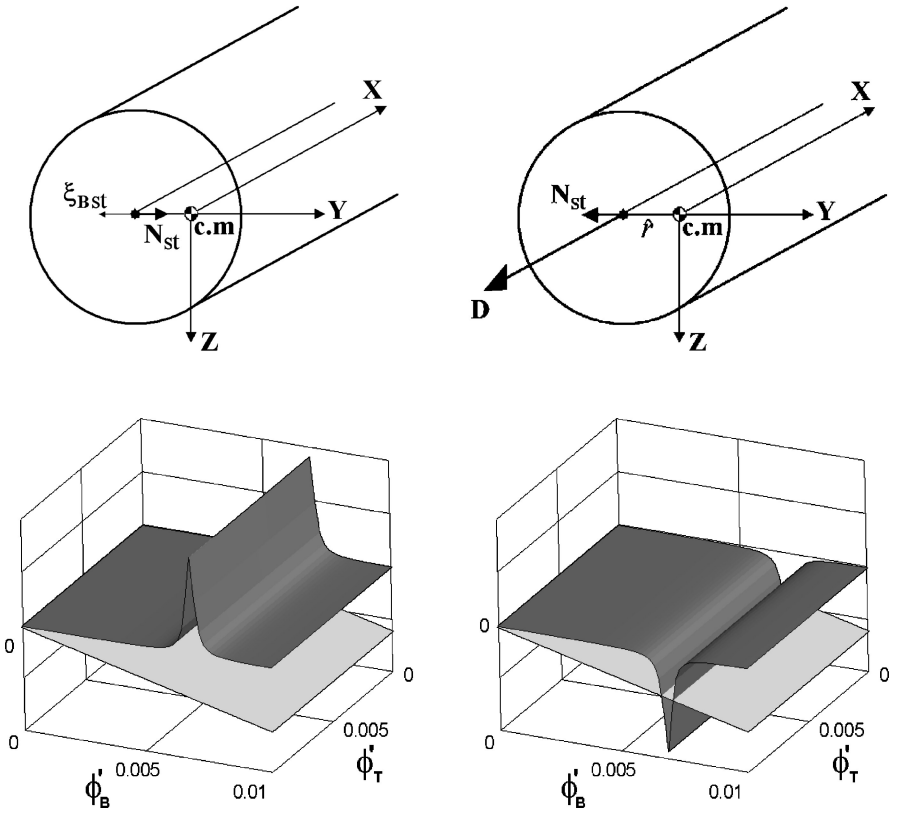

a) **b)**

Fig. 11 Plane and induced roll moment.

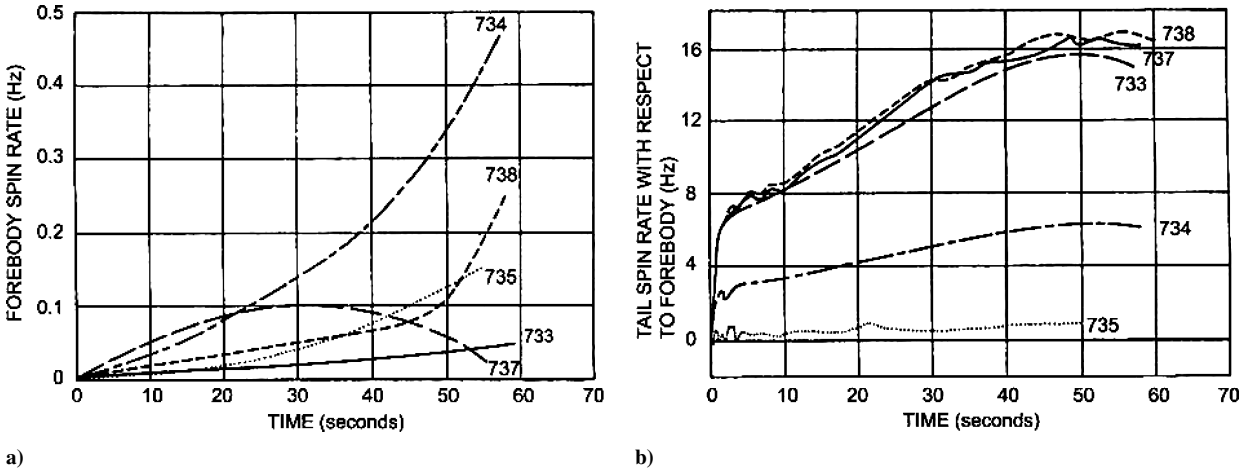

Fig. 13 Free-fall stores for a) body and b) tail rates.

gives rise to several peaks on the tail-induced roll surface, making analysis more complicated.

Comments on Real Flight Behavior

The ability of the present extension of the linear theory to predict actual flight behavior accurately shares the limitations of the linearized motion of fixed-tail configurations. Because of the nonlinear nature of motion, the frequency range of large amplitudes and their magnitude cannot be predicted accurately. Even the notion of resonance has real sense only for linear systems.[16,17] Comparisons with real flight data[10] or with three-degree-of-freedom computations[17] for fixed-tail configurations, although revealing similarities, show up in the inaccuracies of linear theory. The application to free-rolling tail configurations introduces the additional difficulty of two forcing functions. The principle of superposition does not hold for nonlinear systems, and the resulting oscillatory motion contains the exciting frequencies (as in the linear case), plus higher harmonics and combination tones.[16] In spite of these drawbacks, linear theory is the starting point for consistent and comprehensive extensions into the nonlinear range,[17–20] explaining the nature and origin of real flight behavior. Within these limits, linear theory can explain successful flights of free-rolling tail stores and the poor behavior of the same stores with fixed stabilizers.[4] In Ref. 4, real flights of fixed tail bombs (group A) with fin cants ranging from 1.5 up to 3 deg exhibit large amplitude (up to 30 deg) circular yawing motions that persist for up to 6 s after release. In Ref. 9, an explanation of this behavior, characteristic of roll lock-in, is provided for bombs experiencing disturbance oscillations on release. However, the same stores with free-rolling tails perform satisfactorily with oscillations decaying smoothly and rapidly after the release disturbance. Spin histories of the stabilizer and forebodies of the free-rolling tail configurations 733, 734, and 735 are shown in Fig. 13 together with rounds 737 and 738 with monoplane tails. The tail rates of rounds 733 and 734 (with fin cants of 3.4 and 1.4 deg, respectively) quickly accelerate after release to a roll rate well above the pitch frequency (slightly below 1 Hz), whereas the forebody rates show a very slow growth below the pitch frequency. The tail of the round 735 (with only 0.24 deg of fin cant), spins at approximately the pitch frequency from 28 s after release until impact. However, the incidence does not exceed about 1 deg over this period. For these cases, the tail rate passage through resonance does not give rise to large-amplitude oscillations. According to the present extension of the linear theory, this can be explained by the separation between body and tail rates. This margin prevents the coalescence of possibly large trim angles and induced roll moments at the pitch frequency crossing, in contrast with the fixed-tail cases.

Conclusions

This paper presents an analytical treatment of the linear dynamics of free-rolling tail configurations in free flight. A dynamically equivalent fixed-tail rocket is defined, and the effect of asymmetries is introduced by small forcing functions at body and tail rates.

Two resonance conditions appear when crossings of the pitch frequency occur. No significant interference between resonance conditions exists for realistic inertial and rate figures. For practical purposes, the resonance frequency and the associated peak trim angle in one roll channel do not depend on the rate figures of the other. The dynamic effect of the trim angles acting simultaneously results in an epicyclic motion in nonrolling axes. In body- or tail-fixed axes, the total trim angle is the sum of the in-channel fixed component plus the rotary component due to the other channel spinning at the difference between rates.

The bearing friction couples the body and tail roll rates, thus affecting the steady-state conditions. Nonnegligible friction moments are likely to be present in the dry bearings required for long-term storage and military use.

The bearing friction and the proximity between rates can affect body or tail lock-in conditions. The additional degree of freedom separates body and tail lock-in occurrence and represents a comparative advantage for some types of vehicles. This can be exploited through careful tailoring of the pitch frequency crossings.

References

[1]Darling, J. A., "Elimination of the Induced Roll of a Canard Control Configuration by Use of a Freely Spinning Tail," U.S. Navy, Rept. NOLTR 72-197, Aug. 1972.

[2]Blair, A. B., "Remote Control Canard Missile with a Free Rolling Tail Brake Torque System," AIAA Paper 81-0146, Jan. 1981.

[3]Reagan, F. J., and Falusi, M. E., "The Static and Magnus Aerodynamic Characteristics of the M823 Research Store Equipped with Fixed and Freely Spinning Stabilizers," U.S. Navy, Rept. NOLTR 72-291, Dec. 1972.

[4]Reagan, F. J., Shannon, J. H., and Tanner, F. J., "The Joint N.O.L./R.A.E./W.R.E Research Programme on Bomb Dynamics. Part III. A Low-Drag Bomb with Freely Spinning Stabilizers," Australian Defense Science Service, WRE-Rept.-904 (WR&D), June 1973.

[5]Murphy, C. H., "Free Flight Motion of Symmetric Missiles," Ballistic Research Lab., BRL Rept. 1216, Aberdeen Proving Ground, MD, July 1963.

[6]Platou, A. S., "Magnus Force on a Fixed Body," Ballistic Research Lab., BRL Rept. 1193, Aberdeen Proving Ground, MD, March 1963.

[7]Benton, E. R., "Supersonic Magnus Effect on a Finned Missile," *AIAA Journal*, Vol. 2, No. 1, 1964, pp. 153–155.

[8]Nicolaides, J. D., "On the Free Flight Motion of Missiles Having Slight Configurational Asymmetries," Inst. of Aeronautical Sciences, Rept. 395, 1952.

[9]Chadwick, W. R., "Flight Dynamics of a Bomb with Cruciform Tail," *Journal of Spacecraft and Rockets*, Vol. 4, No. 6, 1967, pp. 768–773.

[10]Price, D. A., Jr., "Sources Mechanisms and Control of Roll Resonance Phenomena for Sounding Rockets," *Journal of Spacecraft and Rockets*, Vol. 4, No. 22, 1967, pp. 1516–1525.

[11]Nicolaides, J. D., "Two Non-linear Problems in the Flight Dynamics of Modern Ballistic Missiles," Inst. of Aeronautical Sciences, Rept. 59-17, 1959.

[12]Glover, L. S., "Effects on Roll Rate of Mass and Aerodynamic Asymmetries of Ballistic Reentry Bodies," *Journal of Spacecraft and Rockets*, Vol. 2, No. 2, 1965, pp. 220–225.

[13]Ananthkrishnan, N., and Raisinghani, S. C., "Steady and Quasi-Steady Resonant Lock-In of Finned Projectiles,"*Journal of Spacecraft and Rockets*, Vol. 29, No. 5, 1992, pp. 692–696.

[14]Murphy, C. H., "Some Special Cases of Spin-Yaw Lock-In," *Journal of Guidance, Control, and Dynamics*, Vol. 12, No. 6, 1989, pp. 771–776.

[15]Maple, C. G., and Synge, J. L., "Aerodynamic Symmetry of Projectiles," *Quarterly of Applied Mathematics*, Vol. 6, No. 4, 1949, pp. 345–366.

[16]Stoker, J. J., "Nonlinear Vibrations," *Pure and Applied Mathematics*, 1std ed., Vol. 2, Interscience, New York, 1950, pp. 1–11.

[17]Clare, T. A., "Resonance Instability for Finned Configurations Having Nonlinear Aerodynamic Properties," *Journal of Spacecraft and Rockets*, Vol. 8, No. 3, 1971, pp. 278–283.

[18]Murphy, C. H., "Nonlinear Motion of a Missile with Slight Configurational Asymmetries," *Journal of Spacecraft and Rockets*, Vol. 8, No. 3, 1971, pp. 259–263.

[19]Murphy, C. H., "Subharmonic Behavior of a Slightly Asymmetric Missile," *AIAA Journal*, Vol. 11, No. 6, 1973, pp. 884–885.

[20]Pepitone, T. R., "Resonant Behavior of a Symmetric Missile Having Roll Orientation-Dependent Aerodynamics," *Journal of Guidance and Control*, Vol. 1, No. 5, 1978, pp. 335–339.

R. Cummings
Associate Editor